PR12-16-002

Proposal in Hall C to Jefferson Lab PAC 44 June 6, 2016

Measurement of Parity-violation in the Resonance Region (PVRES) for the Proton and Deuteron

K. Jin, J. Liu, V. Sulkosky† (spokesperson), N. Ton, X. Zheng
University of Virginia, Charlottesville, VA 22901, USA

F. Benmokhtar
Duquesne University, Pittsburgh, PA 15282, USA

P. Markowitz
Florida International University, Miami, FL 33199, USA

D. Biswas, M. E. Christy, B. Dongwi, T. N. Gautam, N. Kalantarians (co-spokesperson), M. Kohl, A. Liyanage, A. Nadeeshani, J. Nazeer, B. Pandey, L. Tang
Hampton University, Hampton, VA 23668, USA

†Contact person, email: vasulk@jlab.org

Abstract

We propose a precise measurement of the parity-violating electroweak asymmetry A_{PV} across the nucleon resonance region and extending into $W > 2$ GeV at $\langle Q^2 \rangle \approx 0.25 - 0.6$ GeV^2 using inclusive scattering of 4.4 GeV longitudinally polarized electrons from unpolarized liquid hydrogen and deuterium targets. The proposal will make use of the new Super High Momentum Spectrometer (SHMS) and the High Momentum Spectrometer (HMS) in Hall C to detect the scattered electrons at a central angle of 10.5°. The uncertainty on the γZ interference radiative corrections, $\Box_{\gamma Z}$, is important to the goals of the Jefferson Lab Q_{weak} measurement, which aims for a 4% determination of the proton's weak charge, and other future planned measurements. Most of the uncertainty in this correction comes from the incomplete knowledge of the γZ structure functions in the low-Q^2 and $W \leqslant 2$ GeV region. New measurements of parity violating electron scattering asymmetries (PVES) on the proton will provide constraints on models and reduce the uncertainty of these structure functions. The measurements on the deuteron will provide information on the isospin dependency of the interference structure functions. Finally, these measurements are of great importance in accurately modeling neutrino interactions, which is essential in the interpretation of neutrino experiments. These new data will also be of use in radiative corrections for the Solenoidal Large Intensity Device (SoLID) PVDIS experiment and will aid in understanding inelastic backgrounds for other PV experiments. We request a total of 25 days for production data taking and 2 days for calibrations and equipment checkout.

Contents

List of Figures

List of Tables

1 Introduction

One of the first pieces of evidence that the proton and neutron have composite structure was the discovery by Estermann and Stern that the proton's magnetic moment was considerably different compared with Dirac's prediction. One may consider this discovery to mark the beginning of hadronic physics, where hadrons are subatomic particles that interact via the strong interaction. A couple of decades later, electron scattering experiments were used to confirm that the nucleon has a spatial distribution. Later on, an extensive study of the nucleon's structure was performed using deep inelastic scattering experiments at the Stanford Linear Accelerator Center (SLAC). From these measurements, it was concluded that the nucleon is composed of point-like particles known as partons, which are now associated with quarks and gluons. Quantum Chromodynamics (QCD) has emerged as the theory that describes the strong interaction of quarks by the exchange of gluons. In the high energy regime, predictions from perturbative QCD have been verified by comparison with experimental results. However, at lower energies, QCD calculations become difficult due to the nature of the strong interaction. Therefore, low-energy effective field theories, models and Lattice QCD are used to make predictions.

A key remaining question is how the transition from partonic to hadronic degrees of freedom occurs. One way to approach this issue is to experimentally investigate the non-perturbative region. Lepton scattering provides a very powerful tool to probe the internal structure of the nucleon, especially since the interactions of leptons are well understood and described by the theory of Quantum Electrodynamics (QED). Jefferson Lab has become the premier facility for measurements using electrons at low and intermediate momentum transfers to study the non-perturbative regime. A wealth of information on the electromagnetic (EM) structure of protons and neutrons has been gleaned from such experiments. However, there is still much to be understood in how to build a nucleon from the fundamental degrees of freedom: quarks and gluons. Besides the EM interaction, the weak interaction also provides another sensitive way to probe the internal dynamics of nucleons and nuclei.

At Jefferson Lab energies, the weak interaction amplitude is considerably smaller than the electromagnetic amplitude. However the parity-violating (PV) part of the weak amplitude is accessible by measuring the beam helicity-dependent asymmetry, A_{PV}. There have been several results utilizing this technique, which include strange nucleon form factors, the radius of the neutron distribution in Pb, and searches for PV extensions to the Standard Model.

The later type of low-energy experiments are at the precision frontier [1–3] and provide an important alternative to high-energy tests of the Standard Model such as those at the Large Hadron Collider.

Most of the previous measurements have focused either on elastic scattering or deep inelastic scattering (DIS) processes. When resonance data is available, the data are mostly taken for background purposes and suffer from relatively large uncertainties. The study of the resonance region for the most part has been neglected, regarding the weak interaction. Due to the different isospin structure and couplings, the weak current will couple to individual resonances differently compared to the EM current. In fact, PVES is more sensitive to the down and strange quarks than the unpolarized structure functions, providing another method to probe these distributions.

The new resonance region data that we propose here will help address the following items:

1. New measurements of A_{PV} on the proton will provide constraints on models and reduce the uncertainty of the γZ interference structure functions. These constraints will improve the uncertainties on current (Q_{weak}) and future measurements via the $\Box_{\gamma Z}$ radiative correction.

2. Measurements on the deuteron will provide information on the isospin dependency of the interference structure functions and complement previous measurements at higher Q^2 [4].

3. These measurements will be of great importance in accurately modeling neutrino interactions, which is essential in the interpretation of neutrino experiments.

4. These new data will also be of use in radiative corrections for the SoLID PVDIS experiment and will aid in understanding inelastic backgrounds for other PV experiments.

5. The precision will allow us to observe resonance structure to the 5% to 10% level and to test and confirm quark hadron duality in the electroweak interaction as seen by Ref. [4].

2 Physics and Motivation

In the Born approximation, the process of lepton-nucleon scattering, including both electromagnetic and weak interactions, occurs by the exchange of a single boson either a virtual photon ($\gamma*$) or a virtual Z boson as shown in Fig. 1. For the remainder of this discussion, the lepton will be specifically referred to as an electron. For an electron with incident energy E, which scatters from a hadronic target with scattered energy E', the energy transferred to the target is given by $\nu = E - E'$. Then $y = \nu/E$ is the fractional energy transferred to the target. With $q = k - k'$ as the virtual photon momentum, $Q^2 = -q^2$ is the four-momentum-transfer squared and represents the virtuality of the exchanged boson.

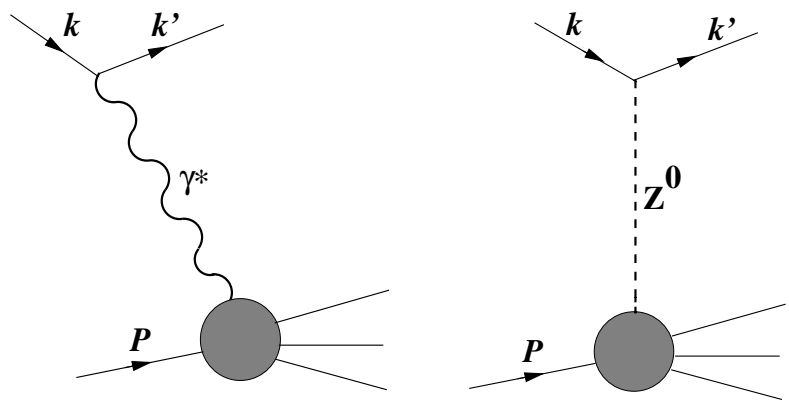

Figure 1: Lowest order Feynman diagrams for inclusive lepton-nucleon scattering, including the electromagnetic (left) and weak (right) interactions. The incident lepton, scattered lepton, and hadron momenta are labeled by k, k', and P, respectively.

2.1 Parity Violating Asymmetries

The differential cross section for electron-nucleon scattering contains electromagnetic (EM), weak and interference contributions. At low energies and small momentum transfers, the weak cross section is significantly smaller than the electromagnetic (EM) cross section, and hence, the former can usually be neglected. The EM part of the cross section is parity conserving, and the cross section is the same for right and left-handed electrons. On the other hand, the electroweak neutral current includes a parity violating contribution, and the electroweak part can be measured using parity violating asymmetries in inclusive polarized electron scattering. The PVES asymmetries A_{PV} for scattering of longitudinally polarized electrons from unpolarized protons or nuclei can be expressed in terms of the cross section difference for right- and left-handed electrons,

$$A_{PV} = \frac{\sigma_+ - \sigma_-}{\sigma_+ + \sigma_-} \,, \tag{1}$$

where σ_h is the cross section for positive helicity ($h = +1$) or negative helicity ($h = -1$). In the case of positive helicity, the electrons are polarized parallel to their momentum, and for negative helicity, anti-parallel to their momentum. In the next sections, we will consider expressions of A_{PV} for both elastic and inelastic electron scattering and the connection between these two processes via the γZ interference structure functions.

2.2 Elastic PVES and the Proton's Weak Charge

The parity violating asymmetry in elastic electron scattering from an unpolarized hydrogen target at small Q^2 can be expressed as [5]

$$A_{PV} = \left(\frac{-G_F Q^2}{4\pi\alpha\sqrt{2}} \right) Q_W^p \,, \tag{2}$$

where G_F is the Fermi constant, and α is the EM fine structure constant. The proton's weak charge (Q_W^p) at tree level is given by $1-4\sin^2\theta_W$ with $\sin^2\theta_W$ being the weak mixing angle. In Eq. (2), a term involving nucleon structure in the form of EM, weak and strange form factors has been omitted, since it is suppressed at low Q^2. The $Q_{\rm weak}$ experiment recently reported the first results on the proton's weak charge [6] with the goal to achieve 4% accuracy for the final results.

For precision extractions of the proton's weak charge one must include radiative corrections, which leads to the following expression of the weak charge [7]

$$Q_W^p = (1+\Delta\rho+\Delta_e)\left(1-4\sin^2\theta_W(0)+\Delta_e^{'}\right)+\Box_{WW}+\Box_{ZZ}+\Box_{\gamma Z}(0). \tag{3}$$

The (0) in Eq. (3) represents the weak mixing angle and γZ contribution at zero momentum. The terms $\Delta\rho$, Δ_e, and $\Delta_e^{'}$ are neutral current corrections and have been previously calculated to the required accuracy [7]. The weak box corrections are indicated by $\Box_{WW}$, $\Box_{ZZ}$, and $\Box_{\gamma Z}$; the terms $\Box_{WW}$ and $\Box_{ZZ}$ can be calculated perturbatively also to the necessary level of precision [8–10].

Recently, the final term in Eq. (3), $\Box_{\gamma Z}$, has received more attention, and this term was discovered to be strongly energy dependent and larger at the $Q_{\rm weak}$ energy (1.165 GeV) than previously expected [11]. This term is sensitive to long-distance physics and is not fully calculable in perturbation theory. The Feynman diagrams for the interference term are shown in Fig. 2. It has two contributions: the vector electron-axial vector hadron coupling,

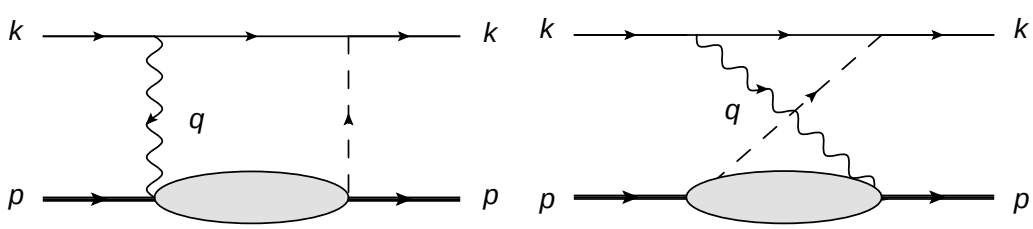

Figure 2: The interference γZ box (left) and crossed box (right) Feynman diagrams. The exchanged γ^* and Z bosons are represented by the wavy and dashed lines, respectively with k the electron momentum, p the hadron momentum, and q the virtual photon momentum. Reproduced from Ref. [12].

$\Box_{\gamma Z}^A$, and the axial vector electron-vector hadron coupling, $\Box_{\gamma Z}^V$ with $\Box_{\gamma Z} = \Box_{\gamma Z}^A + \Box_{\gamma Z}^V$. The former term is important for atomic parity violation experiments, and the later term is important for PVES experiments such as $Q_{\rm weak}$. To evaluate the $\Box_{\gamma Z}^V$ term, dispersion relations have been utilized to obtain the most accurate estimates [11, 13–15]. The different calculations agree with the overall magnitude of the correction but significantly differ in the size of the uncertainty as shown in Table 1. In an effort to reduce the uncertainty, Hall *et al.* [12, 16] constrained the correction using parton distribution functions (PDFs), quark-hadron duality and parity-violating deep-inelastic scattering (PVDIS) data [4, 17, 18], though an uncertainty still exists on the model dependence at low Q^2.

Table 1: Calculations of $\Re e\,\Box^V_{\gamma Z}$ at the kinematics of the Q_{weak} experiment.

Analysis	$\Re e\,\Box^V_{\gamma Z}$ ($\times 10^{-3}$)
Gorchtein *et al.* [15]	5.4 ± 2.0
Rislow *et al.* [14]	5.7 ± 0.9
Hall *et al.* [12]	5.57 ± 0.36

The correction for the Q_{weak} result is about 8%, but the different analyses quote a range of uncertainties from 0.5% up to 2.9% (a factor of ≈ 6) on this value. Gorchtein *et al.* [19] have stated that "It is highly desirable to provide a unified theory uncertainty on this correction before the final analysis of the Q_{weak} experiment is completed." Finally, the uncertainty on this correction can significantly impact the precision goals of future measurements as shown in Table 2, especially for MESA, which aims for a 1% measurement of A_{PV}.

Table 2: Calculations of $\Re e\,\Box^V_{\gamma Z}$ at the kinematics of the Q_{weak}, MOLLER, and MESA experiments from Ref. [16].

Experiment	E [GeV]	$\Re e\,\Box^V_{\gamma Z}$ ($\times 10^{-3}$)
Q_{weak}	1.165	5.4 ± 0.4
MOLLER	11.0	11.2 ± 0.7
MESA	0.18	1.2 ± 0.1

2.3 The γZ Interference Structure Functions

Using dispersion relations, the real part of $\Box^V_{\gamma Z}$ is related to the principal value integral of the imaginary part of the parity violating γZ exchange amplitude, which is dependent on the γZ interference structure functions, $F_i^{\gamma Z}$ [12]. These structure functions are functions of two variables: either taken to be Q^2 and the Bjorken scaling variable $x = Q^2/2p\cdot q$ or Q^2 and the invariant mass $W = \sqrt{M^2 - Q^2 + 2M\nu}$, where M is the nucleon mass. Unfortunately, only limited data exist on $F_1^{\gamma Z}$ and $F_2^{\gamma Z}$ with most of the data at high W (small x) and high Q^2 [20, 21]. However, the dispersion integrals also require crucial input in the low-W and low-Q^2 region, where little data exist. This means that the interference structure functions must be obtained from models and that the calculations of the $\Box^V_{\gamma Z}$ corrections are dependent on the accuracy of these models.

2.3.1 Models of the γZ Interference Structure Functions

A detailed summary of the γZ structure function models is presented in Ref. [12]. Here, we briefly summarize the models and the main contribution to the uncertainties. The virtual

boson-proton cross sections can be conveniently separated into a resonance part and a a non-resonant background contribution. The resonance term includes a sum over prominent low-lying resonances, whereas the background component has been determined by fitting the inclusive scattering data [22, 23]. This separation is model dependent, since the total cross section is the only physical observable. Three of the groups [12, 14, 15] utilize the parameterization of the electromagnetic structure functions in the resonance region by Christy and Bosted [22] in their model. In the fourth analysis [13], the group performed their own fit of the data in the resonance region. The primary difference between all the models is due to how the background contributions for the γZ interference is handled, and this leads to the main source of disagreement between the various estimates of $\Box^V_{\gamma Z}$ and the uncertainty on this correction. The authors of Ref. [19] provide a nice summary of the source of the uncertainties in the background contribution:

- Gorchtein *et al.* (GHRM) have assigned a conservative 100% uncertainty to the background contribution, which is 35% relative to the magnitude of $\Box^V_{\gamma Z}$. This provides the upper limit on the uncertainty of $\Box^V_{\gamma Z}$.
- Hall *et al.*, Adelaide-Jefferson Lab-Manitoba (AJM) model, matched the uncertainty due to the continuum to that of the DIS data at $Q^2 \geq 2.5$ GeV^2 with the assumption that the uncertainty remains constant down to $Q^2 = 0$. They also constrained some of the model parameters, which were previously unconstrained, by using existing world data. They obtained a 6% uncertainty relative to the size of $\Box^V_{\gamma Z}$ This analysis provides the lower limit on the uncertainty of $\Box^V_{\gamma Z}$.
- The uncertainty of the Rislow *et al.* analysis is between the other two and comes from the difference between $SU(4)$ and $SU(6)$ versions of the non-relativistic constituent quark model (NRCQM). However, it isn't clear if all the systematic uncertainties of the NRCQM are taken into account in their estimate.

2.3.2 Inelastic PVES Formalism

At Jefferson Lab beam energies, the main observables sensitive to the interference structure functions are the parity violating asymmetries. In the resonance region, the asymmetry can be written in terms of longitudinal, transverse, and axial PV response functions, which can be decomposed in terms of their isospin content. These response functions are also related to the PV structure functions, and a general expression for A_{PV} for a nucleon or nuclear target in terms of the γZ interference structure functions [12] is given by

$$A_{PV} = g_A^e \left(\frac{G_F Q^2}{2\sqrt{2}\pi\alpha}\right) \frac{xy^2 F_1^{\gamma Z} + \left(1 - y - \frac{x^2y^2M^2}{Q^2}\right) F_2^{\gamma Z} + \frac{g_V^e}{g_A^e}\left(y - \frac{1}{2}y^2\right) xF_3^{\gamma Z}}{xy^2 F_1^{\gamma\gamma} + \left(1 - y - \frac{x^2y^2M^2}{Q^2}\right) F_2^{\gamma\gamma}}, \tag{4}$$

where $F_1^{\gamma Z}$ and $F_2^{\gamma Z}$are the vector γZ interference structure functions, and $F_3^{\gamma Z}$ is the axial-vector γZ interference structure function. $F_1^{\gamma\gamma}$ and $F_2^{\gamma\gamma}$ are the EM structure functions.

Finally, the vector and axial-vector couplings of the electron to the weak current are

$$g_V^e = -\frac{1}{2} + 2\sin^2\theta_W \tag{5}$$

and

$$g_A^e = -\frac{1}{2}\,. \tag{6}$$

2.3.3 Available A_{PV} Resonance Region Data

In Section 2.3, it was mentioned that little data exists in the low-W and Q^2 region. However, in the past few years, some measurements [4, 24, 25] at Jefferson Lab have become available to test and further constrain the models used to determine the $\Box^V_{\gamma Z}$ corrections. The first of these measurements came from the G0 experiment at a Q^2 of 0.34 GeV^2 [25] near the Δ resonance (1.232 GeV). The results are shown in Fig. 3 along with the calculated asymmetries from the GHRM and AJM models in the left- and right-side panels, respectively. Both models agree well with the data point, but the large experimental uncertainty did not enable useful constraints to be placed on the γZ interference structure functions. Clearly the AJM model provides a noticeable smaller uncertainty band than the GHRM model, which is even more pronounced at higher-Q^2 values.

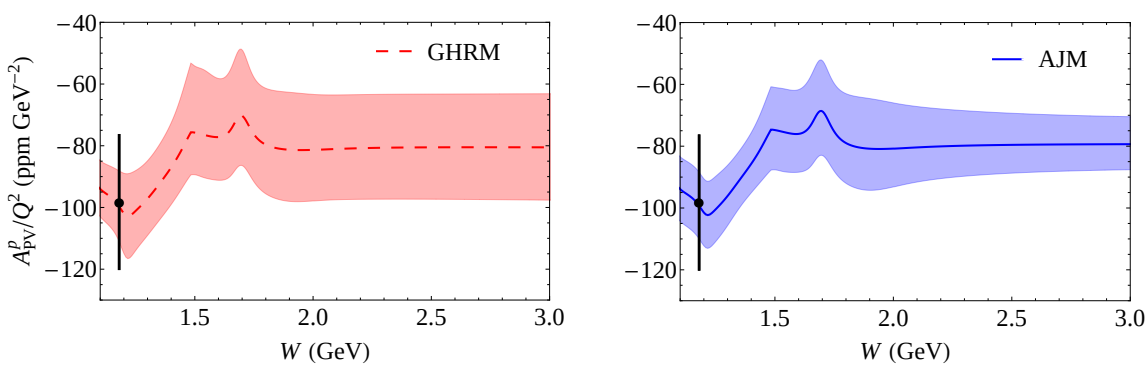

Figure 3: The proton A_{PV} scaled by $1/Q^2$ as a function of W at a fixed beam energy of 0.69 GeV and $Q^2 = 0.34$ GeV^2 for the GHRM model (left) and the AJM model (right). The data (black dot) is from the Jefferson Lab G0 experiment for $W = 1.18$ GeV [25]. Reproduced from Ref. [12].

The best data to compare the calculations and constrain the $\Box^V_{\gamma Z}$ correction is from the Jefferson Lab E08-011 experiment [4, 17, 18]. The main focus of this experiment was to measure the parity violating asymmetry in the DIS region using inclusive electron-deuteron scattering, though they also took data in the resonance region for radiative corrections. A summary of the measured asymmetries with detailed kinematics can be found in Table 1 of Ref. [4]. In Fig. 4, A^d_{PV}/Q^2 is plotted versus W along with various model calculations.

The data in the resonance region were acquired in four kinematic settings, as shown by the different symbols, with average-Q^2 values between 0.76 and 1.47 GeV^2. The vertical error bars indicate the size of the statistical uncertainties, and the horizontal error bars represent the root-mean-square values of the W range for each bin. The shaded bands near the bottom of the figure show the systematic uncertainties from the experimental data. The Matsui *et al.* calculation is only for the Δ region. The calculations from Refs. [12] and [15] are shown by three lines, which show the central values and the upper and lower bounds of the model calculations. Finally, these data are also compared against DIS estimations extrapolated from the CTEQ-Jefferson Lab (CJ) PDF [26] in order to test quark-hadron duality. The uncertainties from the DIS calculation are below 1 ppm and are not discernible. The total

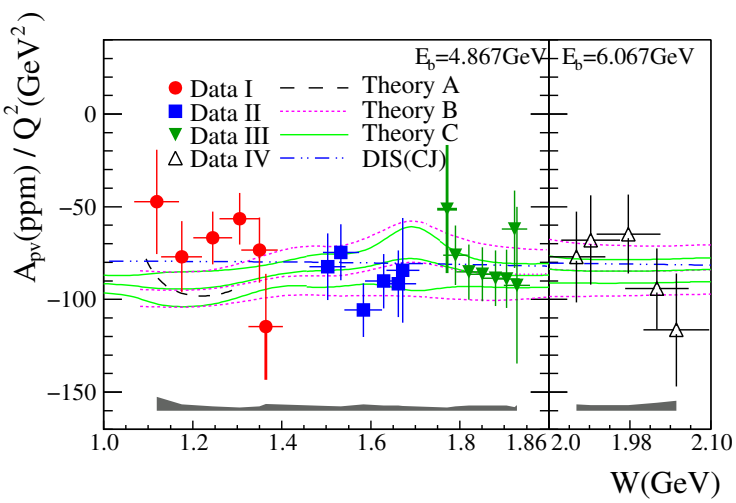

Figure 4: The parity-violating asymmetry from $\vec{e}-^2$H scattering across the resonance region [4]. The data are plotted along with theoretical calculations with theory A [27] (dashed), theory B [15] (dotted) and theory C [12] (solid). The DIS estimation (dash-double-dotted) uses an extrapolation of the CJ PDF [26].

uncertainties on the data range from about 10% to 15%, and the data are consistent with the three model calculations and the DIS estimation within the available precision of the data. Also, no significant resonance structure is seen across the W spectrum. However, for the Δ resonance contribution, these data appear to be systematically off from the theoretical expectations, though both the precision of the data and models are not adequate to make any definitive conclusions. Since these are the best known data in the resonance region, it would be useful to make a precise measurement of the Δ resonance to check these results [28].

Hall *et al.* [12] note that these recent deuterium data have provided confidence in the their procedure of matching to the PDFs at intermediate Q^2 and W. However due to the fact that the deuteron also requires information on both the proton and neutron structure functions, these data unfortunately have limited impact on reducing the uncertainty on the proton $F_i^{\gamma Z}$ structure functions and thus the $\Box^V_{\gamma Z}$ correction. They further go on to state

that dedicated measurements of A_{PV} for the proton would directly constrain the models and lead to the desired reduction in the uncertainty of the radiative correction.

2.4 Quark-Hadron Duality

Bloom and Gilman first observed the feature known as quark-hadron duality in 1970 [29]. Essentially, the low-energy hadronic cross sections averaged over the energy range of the resonance region appear similar to those at high energies in the asymptotic region of partons. This type of duality is known as global duality, since the entire resonance region is considered. When the behavior is observed over limited regions in W for each resonance region, this is referred to as local duality. In particular, the Δ resonance violates local duality. Since the first observation, many other hadronic observables have been found to exhibit this behavior [30], including the unpolarized structure functions $F_2^{\gamma\gamma}$ and $F_L^{\gamma\gamma}$ [31–35] and polarized observables [36–39], though the Q^2 value down to which duality holds varies depending on the quantity in question [4]. Hence, quark-hadronic duality is well established for EM structure function data. The authors of [16] point to experimental evidence that the the isospin dependence of duality and its violation appear to be relatively weak. Hence, it may be reasonable to expect that duality may also hold to a similar level in the electroweak sector for the interference structure functions. The recent data from Wang *et al.* [4] do indeed indicate that duality holds for PVES asymmetries at the (10–15)% level across the resonance region $\left(Q^2 \sim 1\ \mathrm{GeV}^2\right)$, which is comparable to the same level as the EM interaction. The uncertainty mentioned above is only achieved when all the bins in Fig. 4 are averaged separately in each of the four kinematic settings. Hence, the W resolution is somewhat coarse from this data set.

Making the assumption that quark-hadron duality holds for the PV structure functions, the PDF-based description was extended from $Q^2 > 2.5\ \mathrm{GeV}^2$ down to $Q^2 = 1\ \mathrm{GeV}^2$ [16]. The results of this analysis were presented in Table 2. Even if duality is maximally violated ($\approx 14\%$) in the EM structure functions, the increase in the error to $\Re e\,\Box^V_{\gamma Z}$ is $< 0.1\%$. The uncertainty in the analysis leads to a slightly larger model uncertainty, even though the contribution from the resonance region ($Q^2 < 1\ \mathrm{GeV}^2$, $W^2 < 4\ \mathrm{GeV}^2$) to the $\Box^V_{\gamma Z}$ correction has been reduced. This is caused by the more conservative errors applied on $F_1^{\gamma Z}$ and $F_2^{\gamma Z}$ to account for the potential violation of duality.

2.5 Kinematic Regions in Q^2 and W^2

The AJM model defines specific regions in Q^2 and W^2 as displayed in Fig. 5. These regions are particularly useful, since each of them uses different parametrizations to describe the EM excitation spectrum. These are then used to obtain the γZ interference structure functions. Region I includes the resonance region and somewhat beyond: $0 \leqslant Q^2 \leqslant 10\ \mathrm{GeV}^2$ for $W_\pi^2 \leqslant W^2 \leqslant 4\ \mathrm{GeV}^2$ and $0 \leqslant Q^2 \leqslant 1\ \mathrm{GeV}^2$ for $4 < W^2 \leqslant 9\ \mathrm{GeV}^2$. $W_\pi^2 = 1.151\ \mathrm{GeV}^2$ is the invariant mass of the pion production threshold. Region II covers the range $0 \leqslant Q^2 \leqslant$

1 GeV^2 with $W^2 > 9$ GeV^2, and Region III includes $Q^2 > 1$ GeV^2 and $W^2 > 4$ GeV^2. Basically, Region I covers the low-Q^2 and low-W^2 contribution, Region II the low-Q^2 and high-W^2 contribution, and Region III is the high-Q^2 and high-W^2 component.

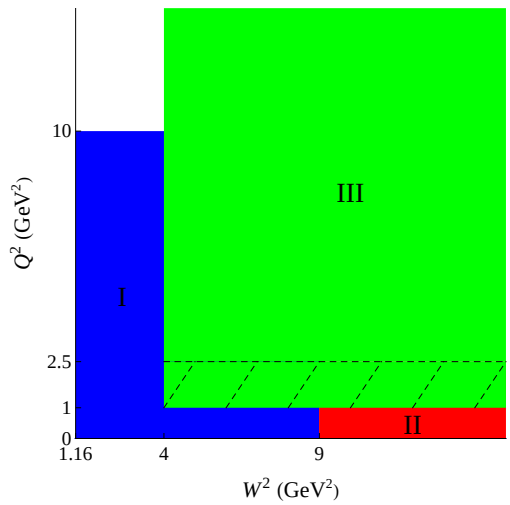

Figure 5: The kinematic regions that contribute to the $\Box^V_{\gamma Z}$ dispersion relation in the AJM model. Region I (blue) consists of the traditional resonance region at low Q^2 and low W^2. Region II (red) includes low Q^2 and high W^2, while Region III (green) is the DIS region extended down to $Q^2 = 1$ GeV^2 by using duality. Reproduced from Ref. [16].

By defining the different regions, we can also examine the energy dependence of the γZ box correction to determine the contribution from each region and the uncertainties on those contributions [16] as illustrated in Fig. 6. At the $Q_{\rm weak}$ incident beam energy (vertical line near 1.165 GeV), Region I contributes about 80% of the sum and dominates the uncertainty, whereas the contributions from Region II and III are only $\approx 7\%$ and $\approx 13\%$, respectively to the total sum. However, as the energy increases, Regions II and III become more important as for the MOLLER experiment [40] at Jefferson Lab. On the other hand for the MESA experiment [41] at Mainz, the majority of the contribution comes from Region I, though the magnitude of the correction is about a factor of 4 smaller than at the $Q_{\rm weak}$ beam energy.

3 Comments from Theorists and the $Q_{\rm weak}$ Collaboration

Although all three models [12, 14, 15] on the γZ box diagram correction to Q_W^P agree well with each other, so far there is no high precision experimental data to prove that the theories and their quoted uncertainties are correct. The first results on $Q_{\rm weak}$ [6] used the constrained analysis of [12] for the γZ box correction, which provides the smallest uncertainties. However,

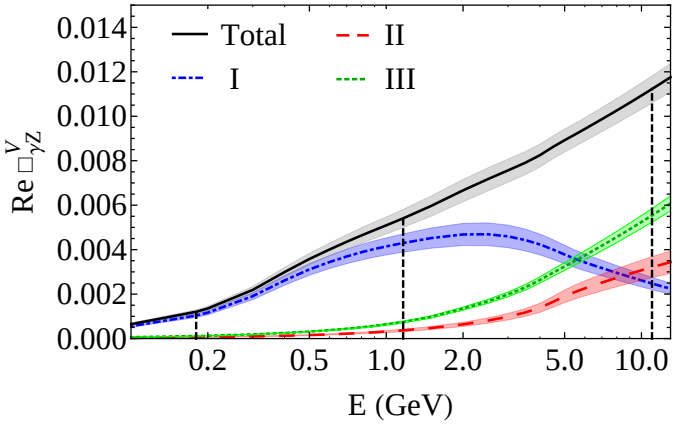

Figure 6: The energy dependence of $\Re e\,\Box^V_{\gamma Z}$ with the beam energies of the PV experiments indicated by the vertical dashed lines: MESA (0.18 GeV) [41], $Q_{\rm weak}$ (1.165 GeV) [6], and MOLLER (11 GeV) [40]. The total (solid) and Region I (dashed-dotted), II (dashed) and III (dotted) contributions are indicated by the different curves. Reproduced from Ref. [16].

as mentioned in Section 2.2, the uncertainties between the three analyses differ by about a factor of 6.

Hall *et al.* [12] indicated in their article that the uncertainties are probably significantly overestimated in Ref. [15]. However, W. Melnitchouk has stated [28] that "we found the largest uncertainty coming form what we call Region I (low Q^2, low W), which gave an uncertainty 7 times larger than that from Region II (low Q^2, high W). Measurements on hydrogen and deuterium would therefore be most valuable in Region I, although any information for high W (or Q^2) would also be valuable in checking the transitions between the regions." In support of the proposal, the AJM Collaboration added these remarks [42]: "Direct measurement of the γZ interference structure functions at low W and Q^2 is extremely important for a number of reasons. While considerable information has been accumulated, largely from Jefferson Lab experiments, on the electromagnetic structure functions of the proton and deuteron, essentially nothing is known about their γZ counterparts in this region. This information is vital in the theoretical estimates of the γZ box corrections to parity-violating elastic scattering experiments, such as Q-weak, which rely on precise knowledge of these backgrounds to extract the fundamental Weinberg angle and test for physics beyond the Standard Model. The weak neutral current provides a unique combination of the quark flavors in the nucleon, which when combined with information from parity-conserving measurements, can be used to reconstruct the flavor and isospin dependence of the nucleon structure in the low-Q^2 regime. This will afford tests of quark-hadron duality, and allow the transition between the DIS and resonance regions to be accurately mapped out for the first time for electroweak interference observables."

M. Gorchtein [43] has commented on the use of quark hadron duality in electroweak

observables and also stated that additional data would be extremely useful: "It is certainly true that the importance of the hadronic boxes sensitive to nucleon and nuclear structure goes beyond $Q_{\rm weak}$. Concerning the duality, it is correct in my understanding that we should not take the duality in γZ interference for granted, especially for real or slightly virtual photons. Several points at a few values of W^2 around 1–5 GeV^2 and a few Q^2 between 0 and 2 GeV^2 for each W^2 would settle this issue for good. Once we have these low-Q^2 points we can use a phenomenological model to connect to the DIS regime. "

From R. Carlini [44], "In the first paper, we used the most recent estimate of the γZ correction available at that time, which was from the AJM Collaboration [12]. Although the correction is large, the uncertainty was about $\sim 0.6\%$. For the final $Q_{\rm weak}$ results, we will use Hall *et al.*'s latest calculations, which from the pre-print has an error of at 0.75% with the same large absolute correction. At this level, the uncertainty due to the γZ will not by a long shot dominate the overall experiment's uncertainty. But of course if it were smaller, it would help and measurements that will constrain it further dispel the myth that one must run an experiment at an ultra low Q^2 to kill the γZ uncertainty."

4 Impact on Neutrino Scattering Measurements

A better understanding of the weak interaction at low Q^2 $\left(0.25 \text{ to } 0.6 \text{ GeV}^2\right)$ is of great importance in understanding low energy neutrino-nucleus interactions, which in turn are needed to determine neutrino masses and couplings through neutrino oscillation experiments [45–48]. Neutrino oscillations in the channel $\nu_\mu \to \nu_\tau$ will be studied by τ production from neutrinos at underground neutrino telescopes like ICECUBE and ANTARES and with long base-line accelerator experiments like MicroBooNE, MINOS, MINERνA, NOνA, and T2K. The future high-accuracy, long baseline neutrino experiment DUNE will require even better knowledge of neutrino-nucleus cross sections. These cross-sections remain the primary systematic for these experiments.

In most experiments, the neutrinos have sufficient energy so that the excitation of nucleon resonances is possible. To go from the τ yield to incident neutrino flux, one needs accurate predictions for the cross section integrated over the neutrino energy spectrum. This involves the three charged current structure functions F_1, F_2, and F_3. Using isospin symmetry, F_1 and F_2 can be related to measurements using inclusive unpolarized electron scattering, and essentially depend on a knowledge of the hadronic vector current. PVES places additional constraints on the structure functions because of the very different weighting of isoscalar and isovector amplitudes compared to unpolarized scattering. Spin-averaged scattering is highly dominated by the u quarks, while PV scattering has relatively strong d quark contributions. Also, PV scattering is somewhat sensitive to the axial nucleon current. Modeling of neutrino-nucleus cross sections requires assumptions such as Partially Conserved Axial Current (PCAC) to relate vector and axial currents that may break down with increasing energy, so experimental constraints from PV scattering are useful [48–51]. The role of duality in the weak current has been discussed in the literature [45, 52, 53], and can be tested

with the present proposal. Our proposed measurements at the 5% level for twelve roughly evenly spaced W values from the pion production threshold through the resonance region and slightly into the DIS region ($W = 2.25$ GeV) will provide powerful constraints on the models used to predict the neutrino cross sections, and complement the direct measurements at MINERνA [45]. In general, electron scattering data is certainly an interesting reaction. One may learn more about the couplings and the hadronic structure of the resonances. A number of neutrino theorists have expressed interest in this proposed measurement data and intend to provide support [54].

5 Planned Parity-Violating Measurements at JLab

Parity-violating precision measurements are an important part of the physics program with the 12-GeV upgraded accelerator. In this section, the experiments and planned proposals related to our proposal are summarized.

5.1 E08-016: The Q_{weak} Experiment

The Q_{weak} experiment [6] aim is to measure the proton's weak charge to 4% accuracy as described in Section 2.2. This experiment also had a special run, where the spectrometer was tuned to the inelastic region at an average $W = 2.23$ GeV and $Q^2 = 0.09$ GeV^2. However, this data has not yet been published, and the kinematics are outside the planned measurements of this proposal. As addressed earlier, the results from our proposed measurement will have a direct impact on constraining the model calculations and their associated uncertainties for the $\Box_{\gamma Z}$ correction in Region I and the transition between Regions I and II.

5.2 E12-11-108: MOLLER Experiment

From the abstract of Ref. [40]: "A highlight of the Fundamental Symmetries subfield of the 2007 NSAC Long Range Plan was the SLAC E158 measurement of the parity-violating asymmetry A_{PV} in polarized electron-electron (Møller) scattering. The proposed MOLLER experiment will improve on the this result by a factor of five, yielding the most precise measurement of the weak mixing angle at low or high energy anticipated over the next decade. This new result would be sensitive to the interference of the electromagnetic amplitude with new neutral current amplitudes as weak as $\sim 10^{-3} \cdot G_F$ from as yet undiscovered dynamics beyond the Standard Model. The resulting discovery reach is unmatched by any proposed experiment measuring a flavor- and CP-conserving process over the next decade, and yields a unique window to new physics at MeV and multi-TeV scales, complementary to direct searches at high energy colliders such as the Large Hadron Collider (LHC)."

The $\Box_{\gamma Z}$ radiative correction also comes into the MOLLER measurement as indicated in

Table 2. In fact, the correction is about a factor of two larger compared to the correction for the Q_{weak} measurement. However, Regions I and II only contribute 50% to the correction for MOLLER, and the uncertainty on the correction is better determined due to the larger contribution from Region III. The proposed measurement will still help to reduce the uncertainty from Regions I and II, which in turn will reduce the overall uncertainty on $\Box_{\gamma Z}$.

5.3 E12-10-007: PVDIS Experiment with SoLID

With the upgrade of the Jefferson Lab electron beam, the PVDIS program will continue with the Solenoidal Large Intensity Device (SoLID) [55]. This device is a multi-purpose spectrometer with physics topics including PVDIS on proton and deuteron targets. The main motivation for the PVDIS experiment is to investigate possible new interactions beyond the Standard Model and to measure the PDF ratio d/u at high Bjorken x. The experiment will obtain data over a wide kinematic range: $x > 0.2$, 2 GeV$^2 < Q^2 <$ 10 GeV^2 and will improve the measurement of the effective weak couplings (C_{2q}) by one order of magnitude compared to the 6 GeV results [17, 18]. According to the addendum of the PVDIS proposal to PAC 35, they "plan to measure the PV asymmetry in the lower W and Q^2 region using lower beam energies" with about 10% of the DIS production time ($\sim$ 17 days). These data will be used to help constrain the radiative corrections to an acceptable level, where the the full radiative correction can be as large as 6% of the measured asymmetry. Figure 7 illustrates the possible resonance region coverage in Q^2 and W for the SoLID PVDIS configuration with incident electron energies between 4.4 and 11 GeV. Though this coverage is in Region I of Fig. 5, the kinematics are at considerably higher Q^2, than planned in our proposal.

The authors of this new proposal looked at using the SoLID apparatus before deciding to move the measurement into Hall C. The main disadvantage with using SoLID at low W and Q^2 is that the minimum angle of SoLID is 22°. This limitation with the smaller Q^2 values reduces the size of A_{PV} and significantly increases the time required to obtain reasonable statistical precision. It was also found that the baffle design for PVDIS hindered the measurements at the lowest beam energy (2.2 GeV), since they are designed to block low energy scattered particles from reaching the detectors. Hall C was chosen over running the experiment in Hall A because the Hall C spectrometers can move to more forward scattering angles and they have a significantly larger momentum bite, which requires fewer momentum settings of the Hall C spectrometers and overall less beam time.

Since SoLID is in the DIS regime, the γZ box correction can be calculated perturbatively, and hence, our proposed measurement is not critical for the SoLID PVDIS experiment for this issue. However, the new measurements will allow for improved radiative corrections for the 12 GeV PVDIS measurement, since our proposed measurements will provide the most precise measurements of A_{PV} at low Q^2 and W in the resonance region.

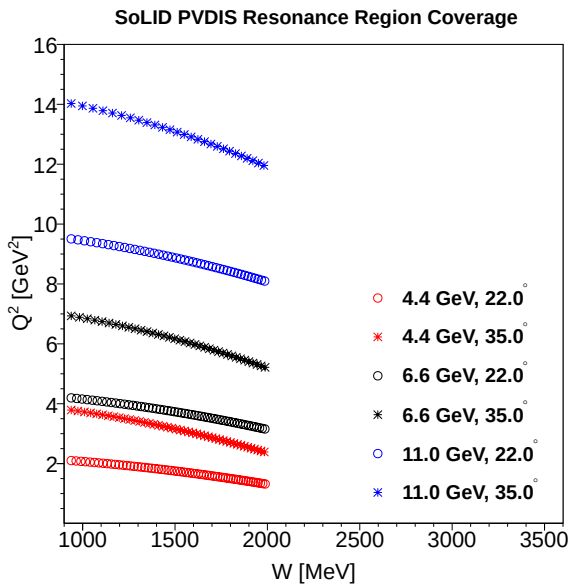

Figure 7: Resonance region coverage for the SoLID PVDIS experiment. The angular coverage for the SoLID PVDIS configuration is between 22° (open circles) and 35° (asterisks) for beam energies of 4.4 GeV (red), 6.6 GeV (black) and 11.0 GeV (blue).

5.4 PR12-14-007: The EMC PVDIS Experiment

From the abstract of the proposal to PAC 42: "We propose to constrain possible flavor-dependent nuclear medium modification effects on quarks using parity-violating deep inelastic scattering on a ^{48}Ca target. This measurement could provide evidence of nuclear parton distribution function modification that is dependent on the isovector nature of a nucleus. Such an effect would represent new and important information on our understanding of nucleon modification at the quark level, which has been know for over 30 years but is still not fully understood theoretically. In addition, such an effect has great importance in the extraction of nuclear parton distribution functions using a variety of techniques and processes, such as using neutrino scattering of Drell-Yan processes. With 60 days of 11 GeV beam at 80 μA using the PVDIS SoLID configuration with a ^{48}Ca target we will obtain 0.8–1.1% statistical precision on the parity violating asymmetry A_{PV} over a range of $0.2 < x < 0.7$ with about 0.7% systematic error." The proposal was deferred by PAC 42, but the spokespersons intend to resubmit an updated proposal to PAC 44.

6 PR06-005: Parity Violating Electron Scattering in Resonance Region (Res-Parity)

Our proposed measurement is closely related to proposal PR06-005, which was submitted to PAC 29 and deferred with regret. That proposal was a resubmission of proposal PR05-005 and PR05-107 with similar physics goals. The spokespersons of PR06-005 planned to measure A_{PV} on three different targets: hydrogen, deuterium and carbon, and would cover the resonance region in the Q^2 range of 0.5–1.0 GeV^2. The physics addressed was related to several important issues: quark-hadron duality, isospin decomposition of the resonances, and the flavor dependence of the EMC effect. It also would have provided important inputs to the neutrino cross sections, and would help other PV measurements such as E158 or PVDIS, regarding backgrounds, higher twist effects and modeling of radiative corrections. The planned measurement used the Hall A base equipment, including a high-rate scaler-based data acquisition system designed and used by the PVDIS 6 GeV experiment [56].

The main issue from the PAC report states: "This PAC felt that the experiment addresses a number of important issues. However, in competition for very limited beam time, no single issue was sufficiently compelling to approve the experiment. The part related to the neutrino physics case would benefit, in a new proposal, from more quantitative arguments and might request inputs from theorists and physicists involved in this field."

7 Experiment and Expected Results

The main goal of this experiment it to measure A_p and A_d in the low-Q^2 and W region to constrain the γZ interference structure functions in order to check and improve model calculations of the $\Box_{\gamma Z}$ radiative corrections for other PV experiments. This planned measurement requires 28 total days in Hall C at Jefferson Lab. This will utilize both of the baseline spectrometers (HMS and SHMS), as well as the standard 20-cm long liquid hydrogen and deuterium targets for production data. Of these 28 days, 19 would be for production running on hydrogen, 5 for production running on Deuterium, and 4 for calibrations and commissioning. The calibration data would consist of data for aluminum and positron backgrounds, and carbon for optics and acceptance studies.

The central angle of both the HMS and SHMS will be positioned to 10.5°. The beam energy requested is 4.4 GeV at 80 μA and 85% longitudinal beam polarization. The fact that the electron beam is not 100% polarized dilutes the experimental asymmetry by the beam polarization, P_b. This measured asymmetry is related to the physics asymmetry by

$$A_{exp} = \frac{N_+ - N_-}{N_+ + N_-} = P_b \cdot A_{PV} \,, \tag{7}$$

where N_+ and N_- are the number of scattered electrons from the + and − helicity states,

respectively. Then the statistical uncertainty is expressed as

$$\delta A = \frac{1}{P_b\sqrt{N_+ + N_-}} \,. \tag{8}$$

Hence, to achieve a few percent statistical uncertainty on a 1×10^{-4} asymmetry requires the detection on the order of 10^{12} electrons. For the kinematics of this proposal, the expected asymmetries are on the order of 10's of parts-per-million (ppm) and are considerably large compared to those measured by the HAPPEX, G0, Q_{weak} and MOLLER experiments at JLab. This in turn reduces the requirements on the beam systematics such as false asymmetries caused by charge, position, and energy. However, theses sources of systematic will still need to be monitored and reduced to acceptable levels.

7.1 Luminosity Monitors

A set of luminosity monitors as used in the G0 experiment [57] placed symmetrically around the beam line will be needed to study and monitor beam-induced fluctuations in the target density. These short-term fluctuations contribute to statistical noise in PV measurements and hence need to be monitored and reduced. By adjusting the operating parameters of the beam and target, the target density fluctuations are reducible to negligible levels. In Hall C, luminosity monitors are not standard equipment. Either previously used monitors from the G0 and Q_{weak} experiments can be reused, or new detectors will need to be built. Typically, these detectors are placed downstream of the target at fairly forward angles; as an example for the G0 experiment, they were located about 2° from the incoming electron beam. Due to the small angles, the physics asymmetry measured by the monitors is quite small. This means that the false asymmetry can be monitored down to $\approx$ 100 ppb, which is negligible compared to the 30–70 ppm asymmetries we plan to measure.

7.2 Parity DAQ

Specialized data acquisition (DAQ) systems [58] have been used both in Halls A and C, which are sometimes referred to as the *parity DAQ*. This system has been used along with a beam helicity feedback system to control beam helicity-dependent false asymmetries for previous PV experiments below the 10^{-7} level. This is accomplished by adjusting the Pockel cell voltage to minimize the beam charge asymmetry. The raw asymmetries also need to be corrected for helicity-dependent fluctuations in the beam parameters such as the positions, angles and energy by using this expression: $A^{bc}_{raw} = A_{raw} - \Sigma c_i \Delta x_i$, where Δx_i represent the measured differences in the helicity window. The coefficients c_i are either determined from the natural jitter of the beam or from data collected when the beam was modulated using steering coils throughout the experiment. For the recent PVDIS experiment [18], the largest of the beam correlated corrections was $\approx$ 0.4 ppm, which is well below our expected statistical precision and other more dominant systematic uncertainties (See Table 4).

7.3 Targets

For the target, we will use two 20-cm long cells one for liquid hydrogen and the other for liquid deuterium with 5 mil thick aluminum end caps for the entrance and exit windows. At Jefferson Lab, different types of target cells have been used for various experiments. In particular, the racetrack-shaped cells (used for in HAPPEX-II) have better cooling flow and are more suitable for PV experiments. However, these cells are difficult to machine. So we propose to instead use a target cell similar to that designed using computational fluid dynamics to minimize density variations for the Q_{weak} [6] experiment, though our target will require a beam heat load power of less than 600 W. Recently, such as cell was designed for the Hall A GMp experiment, and initial boiling studies indicate that the boiling effect for this target is small. In the fall 2016 run period, this target cell will be fully characterized, after which we can make a final determination on which target cell design to use for our measurement. The initial parameters that we will begin with are a 4×4 mm^2 raster and 60 Hz fan speed. The noise from the target density fluctuations will be measured up to 80 μA, and the operating conditions will be optimized based on these measurements. The additional noise added by the target fluctuations are negligible when added to those of the counting statistics [18]. Along with the liquid targets, we also require aluminum dummy targets and a multi-foil carbon optics target.

7.4 Scaler-based DAQ and Deadtime

The planned DAQ system will be similar to the one used for the Hall A PVDIS experiment [56], where the rate for the resonance data was on the order of ≈ 1 MHz. The specialized DAQ included intrinsic particle identification (PID) with the pion contamination being controlled at the level of 2×10^{-4} or below and the electron efficiency was greater than 91%. A simulation known as the Hall A trigger simulation (HATS) was developed to study the deadtime for this system. The systematic uncertainty due to the DAQ deadtime correction on the measured asymmetries was $< 0.5\%$. For the highest electron rate data ($\approx$ 600 kHz), the total deadtime was (2.2–2.6 $\pm$ 0.2)%.

R. Michaels and X. Zheng commented on the scaler-based DAQ in Hall A [59]: "The deadtime and systematic uncertainty will climb approximately linearly with the rate. There may also be some tricks for the design, like avoiding certain modules or avoiding a certain bottleneck. If memory serves me correctly, the dominant deadtime was from the veto electronics because of the high rate from the Cherenkov especially. This was not measured well, and we had to rely mainly on simulation. The veto deadtime was a design mistake, I can recall. It was related to a particular module being *updating* or *non-updating*, meaning whether a second input pulse will reset the deadtime (updating) or not. If it resets, it effectively can prolong the deadtime forever." Hence, it is very likely that the deadtime and uncertainty can be improved upon what was previously achieved.

For the system we plan to build in Hall C, the standard detector signals that we will use

are the gas Cherenkov, two layers of lead-glass and scintillators. Using summing and logic modules, the electron and pion triggers are formed and counted by scalers. Electron and pion triggers identify the respective particle by using different discriminator thresholds for each of the triggers. The scalers that count the triggers and beam charge will be integrated over the helicity period. As was done in Hall A, we plan to divide the both layers of the lead-glass detectors into groups of blocks. The exact number of groups will be optimized by compromising between the rate in the front-end logic modules and the amount of electronics needed. These groups will be formed from the individual block signals by using analog summing modules, and their outputs will be sent to discriminators. Two discriminator widths will be used: a *wide* (100 ns) and a *narrow* (30 ns) width; by comparing the results from these two widths, the deadtime can be estimated. The number of groups will essentially determine our resolution in W, and based on the rate estimates, 100 MeV bins are adequate for our physics goals. We plan to preserve the standard Hall C DAQs to verify the correctness of the trigger and to study backgrounds at low rates, where a complete event analysis will be possible. Finally, we will take advantage of the FADCs in the HMS and SHMS to study high-rate effects such as pileup.

Based on the simulation study from the Hall A PVDIS experiment, we expect to be able to run the proton kinematics at the maximum rate (1.9 MHz) listed in Table 3 with $(8 \pm 0.6)\%$ deadtime. The other proton kinematics will be considerably more manageable. On the other hand, the deuterium rates will be more challenging. Even if the deadtime uncertainty on the asymmetry is reasonable, the effects of pileup need to be considered more careful. We plan on using the HATS simulation to study the proposed kinematics for both the proton and deuterium targets. We expect to have preliminary results before the Program Advisory Committee meets. If needed, we can change the kinematics by slightly increasing the spectrometer angle to decrease the DAQ rates as long as we keep $Q^2 < 1$ GeV^2.

7.5 Rate Estimates

In order to determine the required beam time, a Monte-Carlo simulation (SIMC) of the Hall C spectrometers was utilized. The model of Christy and Bosted [22] provided the EM structure functions to calculate the proton and deuteron cross sections across the acceptances of the SHMS and HMS. The AJM model was used to determine values for the γZ interference structure functions, and those in turn were used to calculate the PV asymmetries (Eq. (4)) for the simulated events. The simulated data for each of the spectrometer momentum settings were then combined together to calculate the rates and average asymmetries in W bins of 100 MeV, using cuts to remove the edges of the acceptance for the two spectrometers. The kinematic settings in W and Q^2 are shown in Table 3 along with the rate estimates for both targets. The π/e ratio is < 0.5 for all proposed kinematics.

E' (GeV)	Q^2 (GeV^2)	W (GeV)	x	rate (MHz)	A (ppm)	dA_{stat} (ppm)
			SHMS LH2			
4.149	0.62	0.938	1.0	0.6	54	2.1
3.208	0.48	1.670	0.20	1.8	39	1.2
2.480	0.37	2.065	0.10	1.0	30	1.6
			HMS LH2			
3.854	0.58	1.216	0.49	1.3	49	1.6
3.314	0.50	1.604	0.23	1.9	37	1.3
2.850	0.43	1.874	0.14	1.2	32	1.6
2.451	0.37	2.079	0.10	0.8	31	2.1
			SHMS LD2			
4.149	0.62	0.938	1.0	1.2	54	2.9
3.208	0.48	1.670	0.20	3.8	44	1.6
2.480	0.37	2.065	0.10	1.2	36	2.8
			HMS LD2			
3.854	0.58	1.216	0.49	2.9	51	2.1
3.314	0.50	1.604	0.23	3.6	43	1.9
2.850	0.43	1.874	0.14	2.4	38	2.3
2.451	0.37	2.079	0.10	1.6	32	2.8

Table 3: Kinematic variables, rate estimates, expected asymmetry (AJM model), and expected statistical uncertainty for the proposed measurements for an incident electron energy of 4.4 GeV and spectrometer scattering angle of $\theta_e = 10.5°$.

7.6 Proton and Deuteron Measurements

The hydrogen data will take the significant portion of the requested time, in order to ensure the desired precision is achieved. Over the 19 days, there would 4 momentum settings for the HMS and 3 for SHMS. This would allow for the intended coverage in W. The deuterium data will take 5 days of the requested beam time. The momentum settings for the HMS and SHMS would be similar to those for the hydrogen production running. This allows for similar coverage in W compared to that of the hydrogen data. The kinematic coverage in Q^2 versus W for the SHMS for both targets is shown in Fig. 8. The coverage is similar for the HMS. The expected relative statistical uncertainties are also shown with 100 MeV bins in W. The deuteron acceptance is truncated due to the fact that we did not have calculations for the AJM model at $W > 2$ GeV to estimate the size of A_d.

Figure 9 shows the expected PV asymmetries divided by the average Q^2 for each W bin for the combined HMS and SHMS. The asymmetries are in units of ppm. The statistical precision varies from 3% to 7% across the resonance region with the highest precision at the Δ resonance. In the final analysis, the size of the W bins will be optimized based on the final statistics recorded.

7.7 Calibration and Commissioning

For the calibration running, approximately 0.5 days each would be needed for positron backgrounds, aluminum backgrounds, and carbon optics. In addition, 2.5 days would be required for general commissioning. Positron running will be valuable for the pair-symmetric backgrounds. The aluminum data will be crucial for subtracting the liquid target cell wall contributions. Optics data will be necessary to understand the acceptance and spectrometer optics.

7.8 Systematics

A break-down of the systematics estimate is given below, in Table 4. In the following sections, the details of the systematic uncertainties are discussed.

Source	Size
Transverse beam pol. (A_n)	$< 2.5\%$
Pole-tip backgrounds	1%
EM radiative corrections	1%
Q^2 Determination	0.9%
Beam polarization	0.9% (using Moller)
False asymmetries	0.5%
Pair-symmetric background	0.5%
Box diagrams	0.5%
Deadtime corrections	$\leq 0.6\%$
Aluminum endcaps	0.4%
Target purity, density fluctuations	0.2%
Pion contamination	$< 0.05\%$
Total	3.3%

Table 4: Table of the estimated systematics for the proposed measurement.

7.8.1 Beam Polarization

We propose to use a 4.4 GeV polarized electron beam with 85% polarization and up to 80 μA of current. The beam polarization will be measured using the Hall C Møller and Compton polarimeters, which achieved uncertainties of 0.85% and 0.59%, respectively, during the recent Q_{weak} experiment. During the 12 GeV era, the Møller is expected to have a 0.9% uncertainty. The Compton uncertainty requires a detailed Monte Carlo study [60] before an estimated uncertainty can be provided. During the measurement, we plan to make periodic Møller measurements, and ideally, the Compton polarimeter will take data along with the production running.

7.8.2 Transverse Beam Polarization

Ideally, the beam polarization will be completely longitudinal. However, usually there is a non-zero polarization in the direction perpendicular to the scattering plane. This effect is highly suppressed for azimuthally symmetric detectors. For small acceptance spectrometers, this is not the case and the correction to the measured asymmetries is given by $\delta A = A_n\left(-S_H \sin\theta_{tr} + S_V \cos\theta_{tr}\right)$, where A_n is the beam-normal asymmetry, $S_{L,H,V}$ are the polarization components in the longitudinal, horizontal, and vertical directions. The vertical angle of the scattered electrons is θ_{tr}, which is usually fairly small ($\sim$ 10 mrads). Hence, $\delta A \approx A_n S_V \cos\theta_{tr}$. For the proposed measurement, we will take dedicated polarimetry measurements to determine S_H and S_V, and we plan to measure A_n for our kinematic points to help constrain this correction and minimize its uncertainty. For our proposal, we quote the value used by [18], where $|S_V/S_L| \leq 2.5\%$.

7.8.3 Experimental Determination of Q^2

The measured asymmetries have a linear relationship with Q^2, and hence, the largest systematic uncertainty from kinematics comes from the knowledge of Q^2 for each W bin. The largest uncertainty that goes into the uncertainty on Q^2 is from the scattering angle. To mitigate this uncertainty, we plan to take carbon optics data at lower currents with the HMS and SHMS drift chambers turned on. Prior to the experiment, we also plan on having alignment surveys of the target ladder, sieve slits and spectrometer angles. From Ref. [18], when survey results are available, the uncertainty on Q^2 was found to be less than 0.9%. For the momentum calibration, we will make use of the large momentum acceptance of the spectrometers and record the location of the *ep* and *ed* elastic peaks, which will serve as a critical cross check on the spectrometer angles and central momentum. Finally, we will also make use of detailed models of the spectrometers, which are the same ones used to generate the rate calculations.

7.8.4 Backgrounds and Contaminations

The raw asymmetries also need to be corrected for various background processes such as events from the aluminum end caps, charged pion production and electrons from pair symmetric processes. The 6 GeV PVDIS experiment [18] measured all these contributions in kinematics similar to our proposal, though at higher Q^2 and W, where they are worse. Hence, we have chosen to take their values as an upper limit to estimate the systematic uncertainties for the proposed measurement. However, we also plan to estimate these contributions for our kinematics and make them available to the Program Advisory Committee, before the presentation.

We have allocated time in our beam time request to measure the contribution of all these sources of background, regarding each of the kinematic settings in Table 3. Using conservative estimates of the uncertainty of model calculations of A_{PV} for aluminum, Wang *et al.* assigned a 0.4% uncertainty on this background for all kinematics. For the charge pion production backgrounds with a pion rejection factor of 4 $\times 10^{-4}$ and the measured pion asymmetries from the dedicated pion trigger, the relative uncertainty on A_{PV} was < 5 $\times 10^{-4}$. We should be able to achieve a similar pion rejection factor for the calorimeters and light gas Cherenkov detectors in the HMS and SHMS, which will keep this uncertainty to an acceptable level. Finally, by reversing the polarity of the spectrometer magnets, the pair-production background can be measured in our proposed kinematics. Wang *et al.* found this contamination to be less than 5 $\times 10^{-3}$ in their DIS kinematics. Since pion production is lower in the resonance region and the pions are produced at lower Q^2, they used this value as an estimate of the uncertainty on this background for their resonance region data. Hence, this is also an upper limit for our measurements.

An additional background that we are working to understand is pole-tip scattering in the Hall C spectrometers. This refers to electrons that scatter from polarized electrons via Møller scattering in the magnetized iron of the HMS and SHMS dipoles. In the Hall A PVDIS experiment, the lead-glass trigger threshold suppressed this background by a factor of 10 compared to previous estimates. They found that without the trigger threshold suppression the upper bound on the contribution was less than 0.3 ppm/A. In Ref. [4], the authors used a more conservative value of $\sim 1\%$ relative uncertainty to the measured asymmetries. We assume the effect will be similar for the dipoles in Hall C, so we have used 1% as the systematic uncertainty until this issue can be further investigated.

7.8.5 Electromagnetic and Box-diagram Radiative Corrections

Radiative corrections need to be applied for the incident and scattered electrons for both internal and external bremsstrahlung and ionization losses. The external corrections can be determined by using the procedure of Mo and Tsai [61]. For the 6 GeV A_d measurements, the uncertainty on the radiative corrections was dominated by the models used in the resonance region for A_{PV}, since the elastic, quasi-elastic and DIS inputs were all based on data with small uncertainties. The model uncertainty was estimated by either taking the difference

between the resonance data and the models or the statistical uncertainty of the measured asymmetries in the resonance region. The larger value of these two options was used as the uncertainty, which resulted in 0.8–3.5% uncertainties on the EM radiative corrections. The largest uncertainty (3.5%) is in the Δ region, where the data show a $\approx 2\sigma$ difference from the models. For the analysis of the proposed measurements, we plan to use a similar procedure as well as several fits to the world data for the unpolarized cross sections and to study the model dependency by using the various γZ structure function models that are now available. The spokespersons of the previous proposal (see Section 6) to measure A_{PV} in the resonance region estimated the systematic uncertainty from the EM radiative corrections to be $\sim 0.5\%$. We have chosen 1% to be more conservative based on the analysis of [18].

The box-diagram radiative corrections are due to effects when the electron exchanges two bosons with the target and are dominated by the $\gamma\gamma$ and γZ box diagrams. For experiment E08-011, these effects were estimated and found to be (0-1)%, and a (0.5 $\pm$ 0.5)% relative correction was applied to the measured asymmetries [4]. Since our kinematics are not too dissimilar to their kinematics, we assume the same size and uncertainty on this correction.

8 Beam Time Request

For this proposal, we request 672 hours (28 days) of beam time to measure the parity violating asymmetries on hydrogen and deuterium targets to the level of 3–7% across the resonance region. Within this time, 24 days are allocated for production running with 19 days on the proton and 5 days for the deuteron. This time estimate also includes 14 hours for measuring the asymmetry from the Al dummy cell to estimate the background from the target end caps and 10 hours on the carbon optics target for spectrometer optics and acceptance studies. We allocate 12 hours for e^+ runs, which is approximately 3 hours at each momentum setting. The remaining 60 hours are dedicated for commissioning of the scaler-based DAQ. Table 5 summarizes the details of the proposed measurement. The kinematics for the SHMS and HMS are run in parallel with three kinematics for the SHMS and four kinematics for the HMS.

9 Summary

We propose to measure in Hall C the parity violating asymmetries A_p and A_d for polarized electron scattering from unpolarized hydrogen and deuterium targets, respectively, across the resonance region and extending into $W > 2$ GeV. The average Q^2 for the measurements will be 0.25–0.6 GeV^2. Assuming an 80-μA polarized beam of 85% beam polarization, we request 28 days of total beam time to reach statistical uncertainties of $\Delta A_{PV}/A_{PV} = 3$–7% with the higher precision achieved at lower W. The estimated systematic uncertainties are less than 3.5%, which is comparable or smaller than the expected statistics. The only new equipment required for this proposal is a scaler-based data acquisition system to achieve the

Target	P (HMS) [GeV]	HMS time [days]	P (SHMS) [GeV]	SHMS time [days]	Total time [days]
LH2	3.854	4.75	4.149	6.33	
LH2	3.314	4.75	3.208	6.33	
LH2	2.850	4.75	2.480	6.33	
LH2	2.451	4.75			
Total LH2					19
LD2	3.854	1.25	4.149	1.67	
LD2	3.314	1.25	3.208	1.67	
LD2	2.850	1.25	2.480	1.67	
LD2	2.451	1.25			
Total LD2					5
Total Production					24
e^+ background					0.5
Al background					0.58
Carbon optics					0.42
Commissioning					2.5
Total					28

Table 5: Beam time request. All data are with a 4.4 GeV electron beam and both the HMS and SHMS spectrometers at 10.5°.

statistical precision and a set of luminosity monitors to monitor the target boiling effect and the false asymmetry. These measurements will provide constraints on models and reduce the uncertainty of the γZ interference structure functions, which will in turn reduce the uncertainty on the $\Box_{\gamma Z}$ radiative corrections for other PV measurements such as Q_{weak}. The measurements on the deuteron will provide information on the isospin dependency of these structure functions. Finally, these measurements are of great importance in accurately modeling neutrino interactions, which is essential in the interpretation of neutrino experiments.

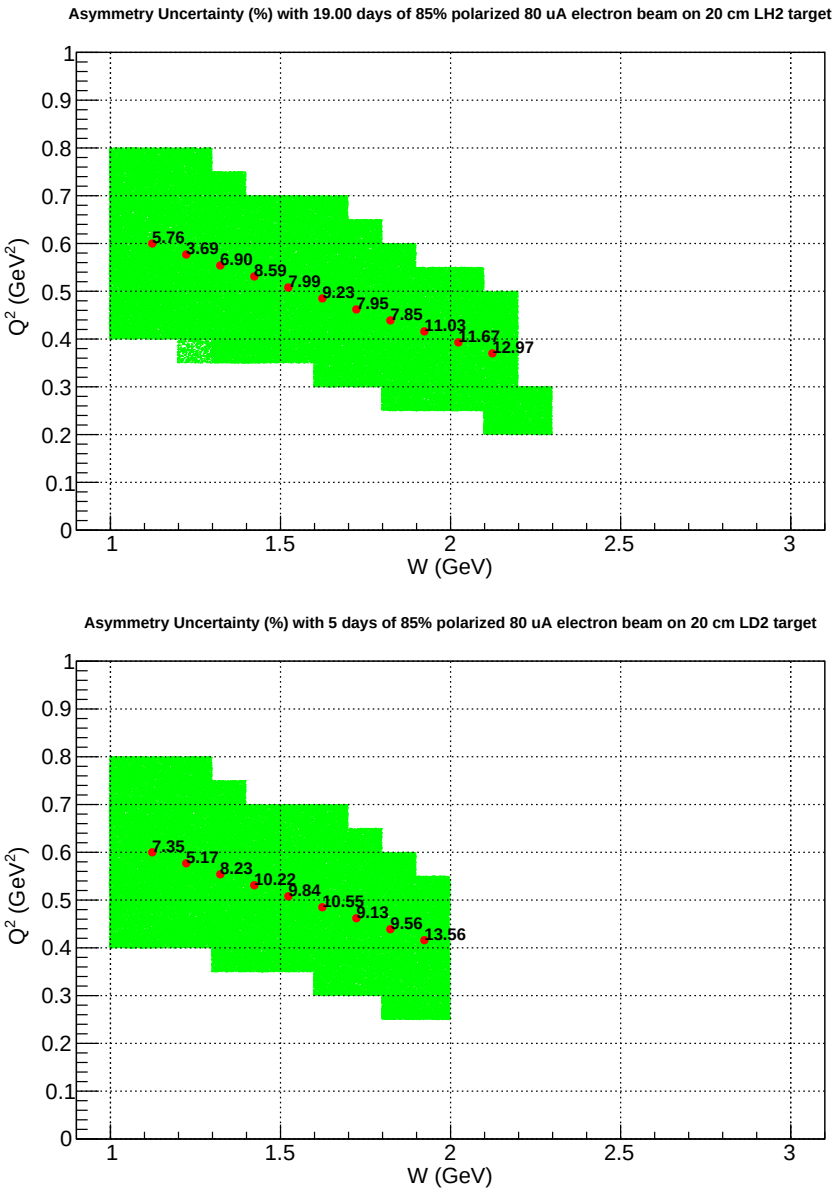

Figure 8: Proposed kinematic coverage for the proton (top) and deuteron (bottom) data with the SHMS in Hall C. The vertical axis represents the four-momentum transfer squared Q^2 in GeV^2 and horizontal axis represents invariant mass W in GeV. The numbers given on the plot represent the estimated, relative errors for the asymmetries.

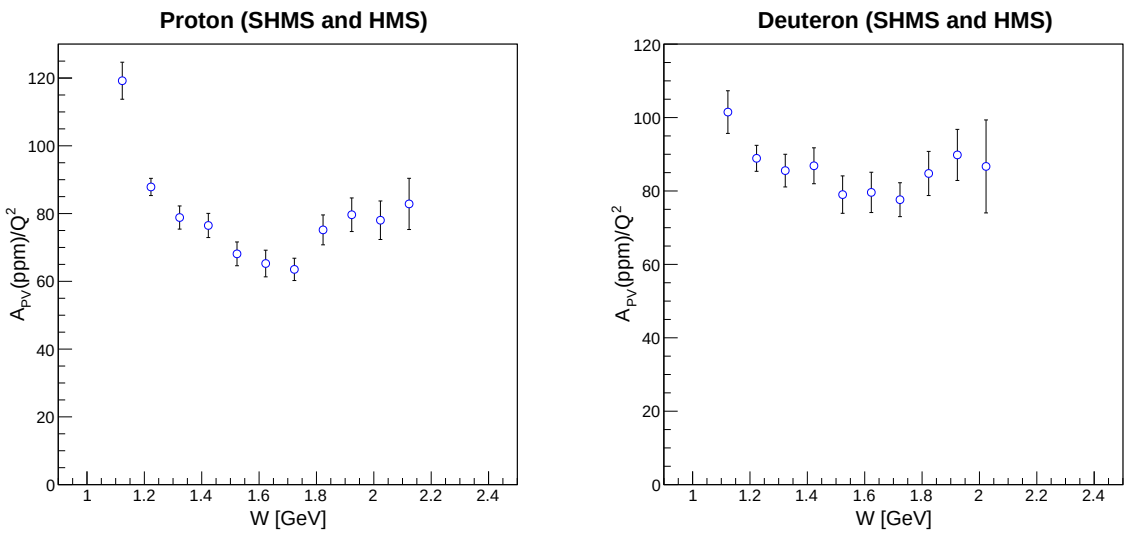

Figure 9: Proposed A_{PV}/Q^2 for the proton (left) and deuteron (right) data versus the invariant mass W in GeV. The error bars represent the expected statistical uncertainties.

References

[1] A. Sirlin and A. Ferroglia, Rev. Mod. Phys. **85**, 263 (2013).

[2] K. S. Kumar, S. Mantry, W. J. Marciano, and P. A. Souder, Ann. Rev. Nucl. Part. Sci. **63**, 237 (2013).

[3] J. Erler and S. Su, Prog. Part. Nucl. Phys. **71**, 119 (2013).

[4] D. Wang et al. (Jefferson Lab Hall A), Phys. Rev. Lett. **111**, 082501 (2013).

[5] M. J. Musolf, T. Donnelly, J. Dubach, S. J. Pollock, S. Kowalski, et al., Phys. Rept. **239**, 1 (1994).

[6] D. Androic et al. (Qweak), Phys.Rev.Lett. **111**, 141803 (2013).

[7] J. Erler, A. Kurylov, and M. J. Ramsey-Musolf, Phys. Rev. **D68**, 016006 (2003).

[8] W. J. Marciano and A. Sirlin, Phys. Rev. **D27**, 552 (1983).

[9] W. J. Marciano and A. Sirlin, Phys. Rev. **D29**, 75 (1984), [Erratum: Phys. Rev. D31, 213 (1985)].

[10] M. J. Musolf and B. R. Holstein, Phys. Lett. **B242**, 461 (1990).

[11] M. Gorchtein and C. J. Horowitz, Phys. Rev. Lett. **102**, 091806 (2009).

[12] N. L. Hall, P. G. Blunden, W. Melnitchouk, A. W. Thomas, and R. D. Young, Phys. Rev. **D88**, 013011 (2013).

[13] A. Sibirtsev, P. G. Blunden, W. Melnitchouk, and A. W. Thomas, Phys. Rev. **D82**, 013011 (2010).

[14] B. C. Rislow and C. E. Carlson, Phys. Rev. **D83**, 113007 (2011).

[15] M. Gorchtein, C. J. Horowitz, and M. J. Ramsey-Musolf, Phys. Rev. **C84**, 015502 (2011).

[16] N. L. Hall, P. G. Blunden, W. Melnitchouk, A. W. Thomas, and R. D. Young, Phys. Lett. **B753**, 221 (2016).

[17] D. Wang et al. (PVDIS), Nature **506**, 67 (2014).

[18] D. Wang et al., Phys. Rev. **C91**, 045506 (2015).

[19] M. Gorchtein, J. Erler, T. Hurth, H. Spiesberger, K. Kumar, M. J. Ramsey-Musolf, and H. B. Meyer (2013), `1311.4586`.

[20] F. D. Aaron et al. (H1), JHEP **09**, 061 (2012).

[21] H. Abramowicz et al. (ZEUS), Phys. Rev. **D87**, 052014 (2013).

[22] M. E. Christy and P. E. Bosted, Phys. Rev. **C81**, 055213 (2010).

[23] P. E. Bosted and M. E. Christy, Phys. Rev. **C77**, 065206 (2008).

[24] D. Androic et al. (G0), Phys. Rev. Lett. **108**, 122002 (2012).

[25] D. Androic et al. (G0) (2012), `1212.1637`.

[26] J. F. Owens, A. Accardi, and W. Melnitchouk, Phys. Rev. **D87**, 094012 (2013).

[27] K. Matsui, T. Sato, and T. S. H. Lee, Phys. Rev. **C72**, 025204 (2005).

[28] W. Melnitchouk, private communication (2015).

[29] E. D. Bloom and F. J. Gilman, Phys. Rev. Lett. **25**, 1140 (1970).

[30] W. Melnitchouk, R. Ent, and C. Keppel, Phys. Rept. **406**, 127 (2005).

[31] I. Niculescu et al., Phys. Rev. Lett. **85**, 1186 (2000).

[32] Y. Liang et al. (Jefferson Lab Hall C E94-110) (2004), `nucl-ex/0410027`.

[33] A. Psaker, W. Melnitchouk, M. E. Christy, and C. Keppel, Phys. Rev. **C78**, 025206 (2008).

[34] S. P. Malace, Y. Kahn, W. Melnitchouk, and C. E. Keppel, Phys. Rev. Lett. **104**, 102001 (2010).

[35] S. P. Malace et al. (Jefferson Lab E00-115), Phys. Rev. **C80**, 035207 (2009).

[36] A. Airapetian et al. (HERMES), Phys. Rev. Lett. **90**, 092002 (2003).

[37] P. E. Bosted et al. (CLAS), Phys. Rev. **C75**, 035203 (2007).

[38] P. Solvignon et al. (Jefferson Lab E01-012), Phys. Rev. Lett. **101**, 182502 (2008).

[39] S. P. Malace, W. Melnitchouk, and A. Psaker, Phys. Rev. **C83**, 035203 (2011).

[40] J. Benesch et al. (MOLLER) (2014), `1411.4088`.

[41] N. Berger et al., in *10th International Workshop on e+e- collisions from Phi to Psi (PHIPSI15) Hefei, Anhui, China, September 23-26, 2015* (2015), `1511.03934`, URL `https://inspirehep.net/record/1404157/files/arXiv:1511.03934.pdf`.

[42] P. G. Blunden, W. Melnitchouk, A. W. Thomas, and R. D. Young (AJM (Adelaide-JLab-Manitoba) Collaboration), private communication (2015).

[43] M. Gorchtein, private communication (2015).

[44] R. D. Carlini, private communication (2015).

[45] D. Harris et al. (2004), `0410005`.

[46] A. Bodek, I. Park, and U. K. Yang, Nucl. Phys. Proc. Suppl. **139**, 113 (2005).

[47] K. Graczyk, C. Juszczak, and J. Sobczyk (2005), 0512015.

[48] E. A. Paschos and J. Y. Yu, Phys. Rev. **D65**, 033002 (2002).

[49] E. A. Paschos, J. Y. Yu, and M. Sakuda, Phys. Rev. **D69**, 014013 (2004).

[50] E. A. Paschos, S. I. Sakuda, M., and J. Y. Yu, Nucl. Phys. Proc. Suppl. **139**, 125 (2005).

[51] S. Kretzer and M. Reno, Phys. Rev. **D66**, 113007 (2002).

[52] R. Belusevic and D. Rein, Phys. Rev. **D38**, 2753 (1988).

[53] C. E. Carlson and N. C. Mukhopadhyay, Phys. Rev. **D47**, 1737 (1993).

[54] E. A. Paschos, I. Schienbien, and J. Y. Yu, private communication (2016).

[55] J. P. Chen, H. Gao, T. K. Hemmick, Z. E. Meziani, and P. A. Souder (SoLID) (2014), 1409.7741.

[56] R. Subedi, D. Wang, K. Pan, X. Deng, R. Michaels, P. E. Reimer, A. Shahinyan, B. Wojtsekhowski, and X. Zheng, Nucl. Instrum. Meth. **A724**, 90 (2013).

[57] D. Androic et al. (G0), Nucl. Instrum. Meth. **A646**, 59 (2011).

[58] K. D. Paschke, Eur. Phys. J. **A32**, 549 (2007), [,249(2007)].

[59] R. Michaels and X. Zheng, private communication (2016).

[60] D. Gaskell, private communication (2016).

[61] L. W. Mo and Y.-S. Tsai, Rev. Mod. Phys. **41**, 205 (1969).